DOI: 10.1002/ejic.200800263

Structure and Shape Evolution of $Bi_{1-x}La_xFeO_3$ Perovskite Microcrystals by Molten Salt Synthesis

Jun Chen,[a] Ranbo Yu,[a] Lihong Li,[a] Ce Sun,[a] Teng Zhang,[a] Houwen Chen,[b] and Xianran Xing*[a,c]

Keywords: Bismuth / Iron / Synthesis design / Perovskite phases / Crystal growth

A facile and environmentally friendly synthesis method has been employed to prepare micron or submicron single-crystal $Bi_{1-x}La_xFeO_3$ with different particle shapes. Various forms of the crystallite are obtained, such as cubic, tetragonal, and semi-sphere crystallites, by means of molten salt synthesis. The thermal stability of $BiFeO_3$ perovskite is greatly enhanced by substitution with $LaFeO_3$. The pure phase of $Bi_{1-x}La_xFeO_3$ can be obtained without the use of the rapid thermal technique by introducing with small amounts of $LaFeO_3$ into $BiFeO_3$. The structure of $Bi_{1-x}La_xFeO_3$ changes from rhombohedral $BiFeO_3$ (*R*3*c*) to orthorhombic $LaFeO_3$ (*Pnma*) with an intermediate orthorhombic phase (*C*222), which is demonstrated by the X-ray diffraction, Raman spectroscopy, and electron diffraction. The formation of $Bi_{1-x}La_xFeO_3$ can be completed in a short time (i.e. 30 min), as the reaction temperature reaches the melting point of NaCl. For the synthesis of $Bi_{0.4}La_{0.6}FeO_3$, the nuclei occur with an irregular tetragonal shape in the initial nucleation stage and then grow with a regular tetragonal profile in the following growth stage. The $Bi_{1-x}La_xFeO_3$ crystal growth was revealed to follow the Ostwald ripening mechanism.

Introduction

$BiFeO_3$ and perovskites based on it (ABO_3) have attracted much attention as multiferroic materials because of their potential applications in new types of electronic devices, such as multiple-state memories and new data-storage media.[1–5] $BiFeO_3$ is well known to be the only multiferroic oxide to date that exhibits both ferroelectric ($T_C \approx 830$ °C) and G-type antiferromagnetic ($T_N \approx 370$ °C) properties above room temperature.[1] The spontaneous polarization of $BiFeO_3$ in heteroepitaxially constrained thin films has been greatly enhanced to almost an order of magnitude higher than that of single crystals.[1] There are still several challenges, such as high leakage, high coercive field, ferroelectric reliability, and weak ferromagnetism, that need to be overcome before the successful application of $BiFeO_3$ as a multiferroic material. In order to resolve these problems, most efforts have recently focused on the specific synthesis techniques[2,6] and partial substitution of $BiFeO_3$ by$A^{2+}B^{4+}O_3$ and $RFeO_3$ (A = Pb and Ba, B = Ti, and R = La, Nd, Pr, etc.).[3–8] In particular, $LaFeO_3$ with an orthorhombic structure (space group *Pnma*) has a homogeneous antiferromagnetic order (T_N = 740 °C) and no ferroelectric order.[9] The multiferroic properties of $BiFeO_3$ have been successfully enhanced by the substitution with non-ferroelectric end member $LaFeO_3$ in the ceramic and film forms.[3–5] In this way, $BiFeO_3$ has achieved the properties necessary for fatigue-free ferroelectric switching, excellent dielectric loss and enhanced remanent polarization and magnetization.[3–5]

For the $Bi_{1-x}La_xFeO_3$ (BLF) multiferroic material, much effort has been focused on films and ceramics,[2–5] and some effective synthesis methods, such as sol–gel,[10,11] hydrothermal,[12] and molten salt synthesis,[13] are available for preparing the end members, especially of $BiFeO_3$. However, as for $Bi_{1-x}La_xFeO_3$ solid solutions, they were mainly obtained by means of the conventional solid-state reaction.[3,14] It is well known that the molten salt synthesis (MSS) is a large-scale, one-step, rapid, and environmentally friendly method for preparing functional materials. In particular, the particle shape depends on the type of salt, surfactant, and composition, and it could be controlled by suitable synthesis conditions.[15] In this study, single phase $Bi_{1-x}La_xFeO_3$, with the whole composition range, was synthesized in a NaCl medium in the temperature range 820–900 °C after a short heating time (2 h). No impurity phases, such as $Bi_{25}FeO_{40}$ and $Bi_2Fe_4O_9$, could be detected in the products prepared by the present MSS method; these impurities are difficult to remove by other methods.[16–18] The crystal structure and

[a] Department of Physical Chemistry, University of Science and Technology Beijing,
Beijing 100083, China
Fax: +86-10-62332525
E-mail: xing@ustb.edu.cn
[b] Department of Materials Physics, University of Science and Technology Beijing,
Beijing 100083, China
[c] State Key Laboratory for Advanced Metals and Materials, University of Science and Technology Beijing,
Beijing 100083, China

phase transition are discussed in detail. The particle shape, interestingly, depends on the composition. Furthermore, the possible crystal growth mechanism is also revealed in this study.

Results and Discussion

The end member $BiFeO_3$ of $Bi_{1-x}La_xFeO_3$ can be synthesized by means of MSS only under very limited sintering conditions, i.e. narrow temperature range of 800 ± 10 °C, rapid heating rate, and quenching process. The formation of single phase $BiFeO_3$ is also influenced by the type of salts.[13] The impurity phases, such as $Bi_{25}FeO_{40}$ and $Bi_2Fe_4O_9$, could be formed due to either thermodynamic preference during the heating process or decomposition of $BiFeO_3$ during the cooling process. The process of rapid heating and quenching favors the formation of pure phase $BiFeO_3$. However, it is important to note that doping with a very small amount of La can be favorable for the formation and for increasing the thermal stability of perovskite phase BLF. For compositions with $x \geq 0.10$, the synthesis of the pure phase of BLF can be carried out at a normal heating rate and does not need the quenching process.

As shown from Figure 1, as-prepared BLF compounds constitute a single phase, and no other impurities such as $Bi_{25}FeO_{40}$ and $Bi_2Fe_4O_9$ could be detected. The XRD patterns can be indexed as single phase in the whole compositional range $0.05 \leq x \leq 1.0$. The structure of BLF evolves from the rhombohedral $BiFeO_3$ (*R*3*c*) to the orthorhombic $LaFeO_3$ (*Pnma*) with an intermediate orthorhombic phase (*C*222).[19] From the evolution of the XRD patterns, it can be clearly seen that the (006) peak at $2\theta = 39.1°$, which is strikingly characteristic of $BiFeO_3$ (*R*3*c*), gradually disappears when $x < 0.2$, and the (111) peak at $2\theta = 25.4°$, which corresponds to $LaFeO_3$ (*Pnma*), appears when $x > 0.6$. The evolution of the phase can also clearly be seen in the enlarged XRD pattern in the 2θ range 45–48° (Figure 1b). The single profile (024) of $BiFeO_3$ splits into two peaks in the range $0.2 \leq x \leq 0.5$, and these two peaks then merge into a single peak at $x \geq 0.6$ with increasing x. For the BLF solid solution, a phase transition occurs at when x is about 0.2 and 0.6. The values of x at the point at which phase transition from rhombohedral to orthorhombic occurs agrees well with those reported for ceramics.[3,14,19]

$Bi_{1-x}La_xFeO_3$ exhibits several phase transitions from end member $BiFeO_3$ to $LaFeO_3$. In particular, the phase transition is more complex in the lower-La-content region ($x < 0.20$). For example, some previous studies suggested that no phase transition occurs and that the rhombohedral structure (*R*3*c*) is maintained when $x < 0.19$;[3,19,20] however, a triclinic P_1 structure was reported in the range $0.06 < x < 0.24$.[21] Thus, in this investigation, a selected-area electron diffraction (SAED) study was performed on BLF with the composition $Bi_{0.90}La_{0.10}FeO_3$ to confirm whether the crystal symmetry is in the rhombohedral or triclinic phase. Two electron diffraction patterns were obtained from the same particle of $Bi_{0.90}La_{0.10}FeO_3$ (Figure 2a,b). These two electron diffraction patterns can be indexed as a rhombohedral structure (*R*3*c*) with a zone axis of $[31\bar{4}0]$ and $[10\bar{1}0]$. The zone axis $[10\bar{1}0]$ was obtained after a rotation of about 19.4° on the tilting axis [0006]. The calculated lattice parameters are $a = b = 5.57(4)$ Å and $c = 13.81(7)$ Å, which are in agreement with literature data.[20] Figure 2 c,d depicts the SAED patterns of a typical individual cube for other $Bi_{1-x}La_xFeO_3$ compositions ($x = 0.05$ and 1.0, respectively). The sharp diffraction spots indicate that the individual cube of BLF is well developed in the single crystal. The SAED patterns of $Bi_{0.95}La_{0.05}FeO_3$ and $LaFeO_3$ could be indexed in the space group *R*3*c* (No.161) and *Pnma* (No. 62), respectively (Figure 2c,d). The calculated lattice parameters are $a = b = 5.57(3)$ Å and $c = 13.83(5)$ Å for $Bi_{0.95}La_{0.05}FeO_3$ and $a = 5.55(4)$ Å, $b = 5.56(4)$ Å and $c = 7.85(3)$ Å for $LaFeO_3$, which are in agreement with the present XRD results and the literature data.[19,20]

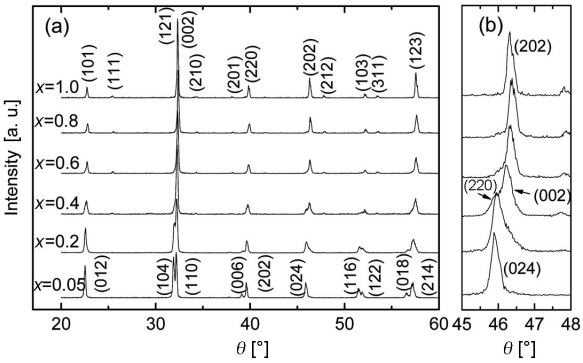

Figure 1. (a) X-ray patterns of $Bi_{1-x}La_xFeO_3$ with x = 0.05, 0.2, 0.4, 0.6, 0.8, and 1.0; (b) the evolution of enlarged X-ray peaks in the 2θ range 45–48°.

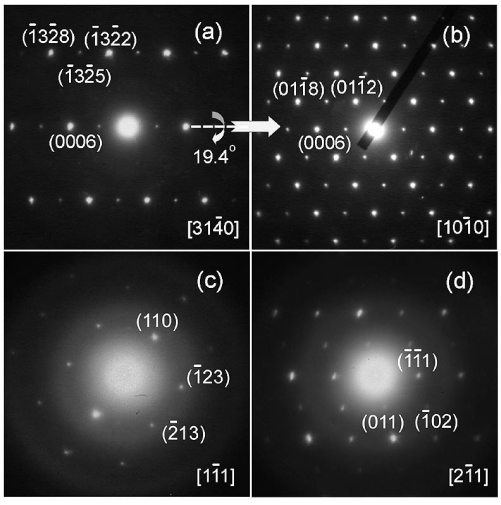

Figure 2. Electron diffraction patterns of $Bi_{1-x}La_xFeO_3$: (a) and (b) show the same $Bi_{0.9}La_{0.1}FeO_3$ particle tilted to the zone axis $[31\bar{4}0]$ and $[10\bar{1}0]$, respectively; pattern (b) is derived from (a) after the rotation of about 19.4° on the tilting axis (indicated by the dash line); (c) $Bi_{0.95}La_{0.05}FeO_3$; (d) $LaFeO_3$.

These phase transitions in BLF are also supported by Raman scattering spectroscopy (Figure 3). At $x < 0.2$, the Raman spectrum is similar to $BiFeO_3$ thin film and ceramic spectra, and the Raman spectrum at $x \geq 0.6$ shows a similar character to that of $LaFeO_3$.[3,22] However, the Raman spectra for $0.2 \leq x \leq 0.5$ are very different from those of end member $BiFeO_3$ and $LaFeO_3$. In the rhombohedral phase ($x < 0.2$), the Raman spectra of BLF with $x = 0.05$ and 0.10 show negligible LO–TO splitting with A_1 symmetry in the lower frequency region, which indicates that the short-range interatomic force dominates the long-range force in the bulk state of BLF, in contrast with that in epitaxial films of $BiFeO_3$.[22] The optical modes of three A_1 modes (labeled by A_1-1, A_1-2 and A_1-3), as well as E(1TO) and E(2TO), which are dominated by the covalent Bi–O bonds, show a slightly downward shift with increasing La content. According to the simple harmonic model [Equation (1)], the A_1 and E(TO) modes should shift upwards because of substituting lighter La atoms for heavier Bi atoms; however, these optical modes shift inversely with increasing La content, which indicates the softening of the force constant k between the Bi–O bonds. Substitution of Bi by La weakens the strong hybridization between Bi ($6s^26p^3$) and O ($2s^22p^4$). As the La content increases to $x = 0.2$, a pronounced change appears in the Raman spectrum. Several new active modes appear, such as those at 106.8 and 623.7 cm^{-1}, and the A_1-1 mode abruptly shifts upwards. As the La content continues to increase to $x = 0.6$, another phase transition occurs between the two orthorhombic phases, with the disappearance of the mode A_1-2 and A_1-3. In $Bi_{1-x}La_xFeO_3$, the structural phase transformations at $x = 0.2$ and 0.6, revealed by the Raman spectra, agree well with those revealed by the XRD investigations.

$$\omega = \sqrt{k/m^*} \quad (1)$$

where ω is the mode frequency, k is the force constant, and m^* is the reduced mass of optical mode.

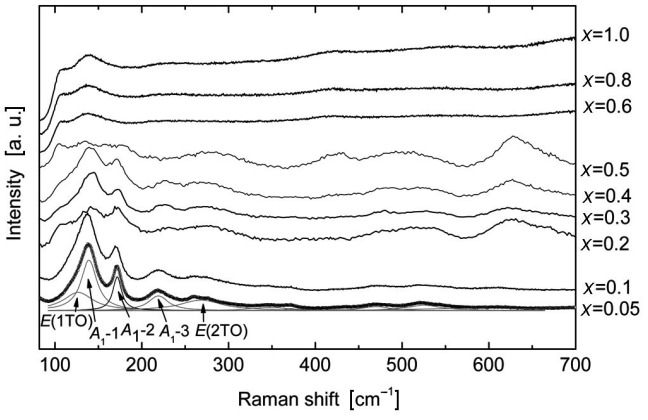

Figure 3. Raman scattering patterns of $Bi_{1-x}La_xFeO_3$ with the composition $0.05 \leq x \leq 1.0$. The positions of active modes of $Bi_{1-x}La_xFeO_3$ ($x = 0.05$ and 0.10) are calculated by full-pattern fitting with the Lorentzian line.

Figure 4 presents the SEM images of the BLF crystallites. It can be seen that BLF with $x = 0.05$, 0.2, and 0.4 mainly consists of cubic crystallites with truncated edges and corners (inset of Figure 4b). The average size is about 1 μm. For $x = 0.6$, the particle shape changes to a tetragonal crystallite with flat faces, sharp corners and well-defined edges (inset of Figure 4d). However, as x increases to 0.8 and 1.0, the particle shape markedly evolves into a semisphere, and the size of particle is ca. 300 nm. It could be concluded that the particle shape and size of BLF depend on the composition. Such a dependence of particle shape on the composition is also found in the perovskite $Ca_{1-x}Sr_xTiO_3$ prepared by MSS.[15b] The shape can be further controlled by investigating the effects of different types of salts and surfactants. As shown in Figure 4, some small particles adhere to large ones, which indicates that the growth of BLF could follow the Ostwald ripening mechanism.[23] After the formation of BLF, the smaller particles gradually dissolve into the NaCl flux, and then redeposit onto the larger particles. Furthermore, during the cooling process, the dissolved BLF in the NaCl flux precipitates as very fine particles adhering to the large particles. This crystal growth mechanism is also directly supported by the HRTEM measurement, which will be discussed in the following paragraph.

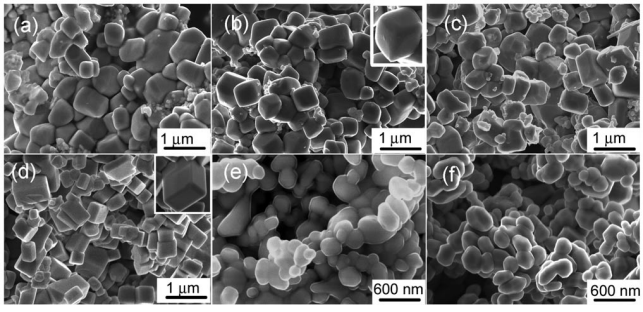

Figure 4. SEM images of $Bi_{1-x}La_xFeO_3$: (a) $Bi_{0.95}La_{0.05}FeO_3$; (b) $Bi_{0.8}La_{0.2}FeO_3$; (c) $Bi_{0.6}La_{0.4}FeO_3$; (d) $Bi_{0.4}La_{0.6}FeO_3$; (e) $Bi_{0.2}La_{0.8}FeO_3$; (f) $LaFeO_3$. The insets show the shape of an enlarged particle.

As shown from Figure 5, the EDS analysis confirms that the chemical composition $Bi_{0.95}La_{0.05}FeO_3$ agrees with the nominal ratio. The elements of Cu and C originate from the TEM grid. A further high-resolution TEM (HRTEM) image of $Bi_{0.95}La_{0.05}FeO_3$ reveals the nature of the single crystal. The interplanar spacing of about 2.83 Å corresponds to the (104) plane of $Bi_{0.95}La_{0.05}FeO_3$. It is important to note that the thin border of the $Bi_{0.95}La_{0.05}FeO_3$ cube is in the amorphous form, while the inside is in the single-crystal form, which can clearly indicated by Fourier transform (Figure 5b). The electron diffraction in the area 1 shows the amorphous ring, whereas the electron diffraction in the area 2 shows the sharp diffraction spots (insets, Figure 5b). The dissolved BLF in the NaCl flux first deposits onto the surface of the large particles in the amorphous form, and then gradually crystallizes with increasing

sintering time. The growth of the BLF crystal follows the Ostwald ripening mechanism, as confirmed by the present HRTEM investigation.

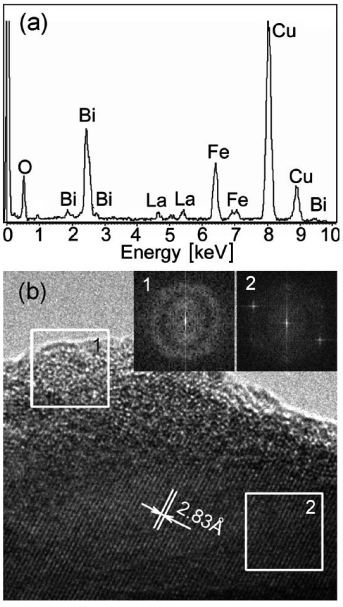

Figure 5. (a) EDS pattern and (b) HRTEM image of a typical individual nanoparticle of $Bi_{0.95}La_{0.05}FeO_3$. The insets are SAED patterns of area 1 and 2 by Fourier transform.

It is important to note that the particle shape and size are also different in the nucleation and growth stages, as has recently been found in the preparation of $BaZrO_3$ perovskite particles in NaOH/KOH medium by means of MSS.[24] What will be the particle shape of BLF in these two stages? For the BLF perovskite, $Bi_{0.4}La_{0.6}FeO_3$ (BLF60) was selected to study this effect because of its relatively uniform tetragonal shape (Figure 4d). In order to differentiate the two stages of nucleation and growth, a series of samples (1–9) corresponding to successive temporal stages during the formation process of BLF60 (heated at a rate of 5 °C min^{-1} to 850 °C and then kept at this temperature for 240 min) were synthesized. The samples 1–9 were taken out of the furnace and cooled to room temperature in air. Figure 6 depicts the reaction-time dependence on the furnace temperature, the weight percentage of BLF60 (χ_w), and the average particle size for the BLF60 sample. The weight percentage of BLF60 was calculated on the basis of the main XRD peak intensity of each phase, which is defined as follows [Equation (2)].

$$\chi_w = I_{BLF60}/(I_{BLF60} + I_{Bi_2O_3} + I_{La_2O_3} + I_{Fe_2O_3}) \quad (2)$$

where I is the main XRD peak intensity of each phase.

The average particle size was determined by statistical analysis of tetragonal particles on the basis of the SEM images. As shown from Figure 6, the starting oxides (Bi_2O_3, La_2O_3, and Fe_2O_3) do not react in the NaCl medium when the furnace temperature is below 600 °C because the reaction temperature is far below the melting point of NaCl (801 °C). As the reaction temperature rises up to the melting point of NaCl, the reaction of raw oxides is rapidly accelerated and the weight percentage of BLF60 largely increases from 6.2% (sample 2) to 77.2% (sample 4) (Figure 6b). The chemical reaction to form BLF60 can be completed in a very short reaction time, i.e. 30 min, from sample 2 to 6. Upon heating the initial mixture, the starting oxides dissolve into the NaCl molten salt, react, and then gradually form BLF60. With increasing reaction time, nucleation occurs as the supersaturated solute concentration of BLF60 reaches the critical solubility (C^{nu}_{min}), which is above the equilibrium solubility (C_0).[24] Once nucleation occurs, growth of the particles takes place simultaneously. However, as the concentration is below C^{nu}_{min} in the following reaction process of raw materials, nucleation stops, and the existing nuclei continue to grow. As shown in Figure 6b, this stage can be regarded as the growth stage without nucleation (sample 6–9), where the formation of BLF60 is complete and no raw oxides exist in the NaCl molten salt for further nucleation. For samples 1–5, nucleation and particle growth take place simultaneously. In this stage, once nucleation occurs, the particle size of sample 2 increases to ca. 200 nm

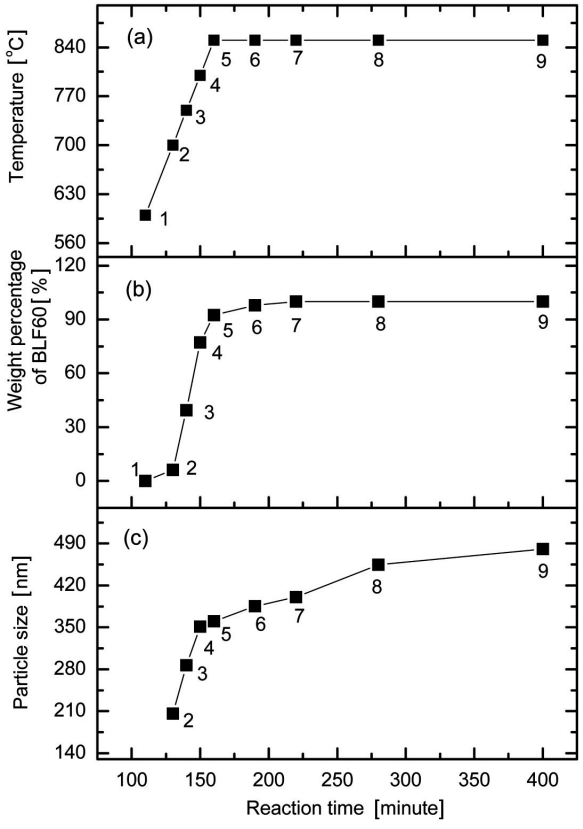

Figure 6. (a) Furnace temperature, (b) weight percentage of $Bi_{0.4}La_{0.6}FeO_3$, and (c) average particle size as a function of reaction time for $Bi_{0.4}La_{0.6}FeO_3$. The numbers represent the sample of $Bi_{0.4}La_{0.6}FeO_3$ heated at different reaction times.

(Figure 6c). The particle size increases rapidly in the initial stage of BLF60 formation (i.e. samples 2–5) and then gradually increases in the following growth stage (i.e. samples 6–9).

Figure 7 shows SEM images at the different stages of BLF60 formation. During the stage where nucleation is dominant for sample 3 (weight percentage of BLF60 is 39.4%), the particle has an irregular tetragonal crystallite shape (Figure 7a). As the reaction time is increased, the particles gradually grow into a regular tetragonal crystallite with sharp corners and straight edges (sample 9, weight percentage of BLF60 is 100%; Figure 7c). The clear profile of the particles indicates a relatively low solubility of BLF60 in the NaCl molten flux, which could also be supported by the relatively slow growth rate during the particle growth stage of the tetragonal particle (samples 6–9 shown in Figure 6c). The relatively low solubility of BLF60 does not accelerate the particle growth. In fact, the average size increases only by ca. 25% from sample 6 to 9. After the completion of the reaction of precursor oxides, the growth of particles is controlled by the Ostwald ripening mechanism (samples 6–9),[23] where the smaller particles gradually dissolve into the NaCl molten flux and the larger ones grow. It should to be noted that the particle growth behavior of $BaZrO_3$ is different from that observed in this study. The particle size of $BaZrO_3$ is similar in the predominantly nucleation stage before the formation of $BaZrO_3$ is complete; however, the size grows rapidly in the following particle growth stage. The particle shape is also different in these two formation stages; cubic particles are formed in the initial stage, which then transforms into spheres with increasing reaction time.[24] Apart from the different nature of the perovskites, this difference in particle growth behavior observed in the present study and that reported in the literature could arise from the different types of molten salts. The temperature-dependent properties of the molten salt, such as melting point, viscosity, and solubility, will play an important role in the particle size and shape.

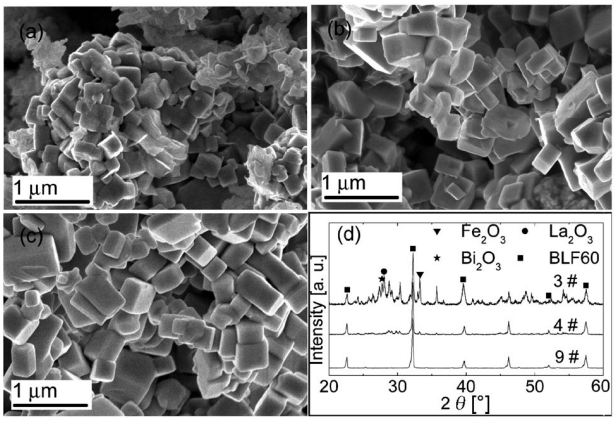

Figure 7. SEM images for tetragonal-shaped particles of $Bi_{0.4}La_{0.6}FeO_3$ at different reaction times: (a) sample 3, 130 min; (b) sample 4, 140 min; (c) sample 9, 400 min. (d) X-ray diffraction patterns corresponding to these three samples, where the main peaks for the raw materials are indicated by symbols.

Conclusions

$Bi_{1-x}La_xFeO_3$ of micron or submicron single-crystals are prepared by a facile, one-step, and environmentally friendly molten salt synthesis. The particle shape, which include cubic, tetragonal, and semi-sphere crystallites, evolves with composition. The structure changes from rhombohedral $BiFeO_3$ (*R*3*c*) to orthorhombic $LaFeO_3$ (*Pnma*) with an intermediate orthorhombic phase (*C*222), which were revealed by the XRD, Raman scattering spectroscopy, and electron diffraction. $Bi_{1-x}La_xFeO_3$ exhibits the rhombohedral symmetry at $x < 0.20$. For $Bi_{0.4}La_{0.6}FeO_3$ with a tetragonal shape, nucleation is completed in a short time as the reaction temperature nears the melting point of the NaCl salt. The tetragonal particle size increases rapidly in the initial stage of $Bi_{0.4}La_{0.6}FeO_3$ formation, while it only gradually increases in the following growth stage. In all temporal stages, $Bi_{0.4}La_{0.6}FeO_3$ exhibits a tetragonal shape. The Ostwald ripening mechanism plays an important role in the crystal growth of $Bi_{1-x}La_xFeO_3$. The present simple method could be useful for large-scale synthesis of other important multiferroic materials and for the control of the crystal shape under suitable preparation conditions.

Experimental Section

$Bi_{1-x}La_xFeO_3$ was synthesized in the whole composition range $0.05 \leq x \leq 1.0$ with a 0.1-step and spans several structural transitions from rhombohedral $BiFeO_3$ (*R*3*c*) to orthorhombic $LaFeO_3$ (*Pnma*). In a typical reaction, Bi_2O_3, La_2O_3, Fe_2O_3, and NaCl were mixed, with a molar ratio of oxides according to the composition $Bi_{1-x}La_xFeO_3$ and a molar ratio for BLF/NaCl 1:3. The mixture was ground in ethanol for 20 min. After the mixture was dried, it was transferred to a crucible, and then loaded into a furnace. The pure phase of BLF can be obtained after heating the mixture at 820–900 °C for 2 h and washing the mixture several times with deionized water to remove the NaCl salt. It is important to note that for the synthesis of BLF at the low values of x ($x \leq 0.05$), a process such as the rapid-thermal technique[2,3] needs to be introduced to maintain the single phase of BLF. The detailed experimental process can be found in our recent report.[13] For the synthesis of $Bi_{1-x}La_xFeO_3$ with a higher content of La ($0.10 \leq x \leq 1.0$), a normal heating process can be used. The morphology and structure of the BLF samples were characterized by scanning electron microscopy (SEM, model: LEO1530, LEO Electron Microscopy Ltd., Germany), high-resolution transmission electron microscopy (HRTEM, model: JEM-2010, JEOL, Japan), and X-ray diffraction (XRD, model: M21XVHF22, Mac Science, Yokohama, Japan). Raman scattering data were collected by using a Raman spectrometer (model: JY-T64000, Jobin Yvon, France).

Acknowledgments

This work was supported by the National Natural Science Foundation of China (No. 50725415, 20731001, and 50374009) and the Funds of Ministry of Education of China for PCSIRI.

[1] J. Wang, J. B. Neaton, H. Zheng, V. Nagarajan, S. B. Ogale, B. Liu, D. Viehland, V. Vaithyanathan, D. G. Schlom, U. V. Wagh-

mare, N. A. Spaldin, K. M. Rabe, M. Wuttig, R. Ramesh, *Science* **2003**, *299*, 1719–1722.
[2] S. T. Zhang, M. H. Lu, D. Wu, Y. F. Chen, N. B. Ming, *Appl. Phys. Lett.* **2005**, *87*, 262907.
[3] S. T. Zhang, Y. Zhang, M. H. Lu, C. L. Du, Y. F. Chen, Z. G. Liu, Y. Y. Zhu, N. B. Ming, X. Q. Pan, *Appl. Phys. Lett.* **2006**, *88*, 162901.
[4] D. Lee, M. G. Kim, S. Ryu, H. M. Jang, S. G. Lee, *Appl. Phys. Lett.* **2005**, *86*, 222903.
[5] Y. H. Lee, J. M. Wu, C. H. Lai, *Appl. Phys. Lett.* **2006**, *88*, 042903.
[6] G. L. Yuan, S. W. Or, *Appl. Phys. Lett.* **2006**, *88*, 062905.
[7] J. S. Kim, C. I. Cheon, C. H. Lee, P. W. Jang, *J. Appl. Phys.* **2004**, *96*, 468–474.
[8] N. Wang, J. Cheng, A. Pyatakov, A. K. Zvezdin, J. F. Li, L. E. Cross, D. Viehland, *Phys. Rev. B* **2005**, *72*, 104434.
[9] J. Lüning, F. Nolting, A. Scholl, H. Ohldag, J. W. Seo, J. Fompeyrine, J.-P. Locquet, J. Stöhr, *Phys. Rev. B* **2003**, *67*, 214433.
[10] F. Chen, Q. F. Zhang, J. H. Li, Y. J. Qi, C. J. Lu, X. B. Chen, X. M. Ren, Y. Zhao, *Appl. Phys. Lett.* **2006**, *89*, 092910.
[11] T.-J. Park, G. C. Papaefthymiou, A. J. Viescas, A. R. Moodenbaugh, S. S. Wong, *Nano Lett.* **2007**, *7*, 766–772.
[12] J. T. Han, Y. H. Huang, X. J. Wu, C. L. Wu, W. Wei, B. Peng, W. Huang, J. B. Goodenough, *Adv. Mater.* **2006**, *18*, 2145–2148.
[13] J. Chen, X. R. Xing, A. Watson, W. Wang, R. B. Yu, J. X. Deng, L. Yan, C. Sun, X. B. Chen, *Chem. Mater.* **2007**, *19*, 3598–3600.
[14] Q. H. Jiang, C. W. Nanw, Z. J. Shen, *J. Am. Ceram. Soc.* **2006**, *89*, 2123–2127.
[15] a) Y. B. Mao, S. Banerjee, S. S. Wong, *J. Am. Chem. Soc.* **2003**, *125*, 15718–15719; b) Y. B. Mao, S. S. Wong, *Adv. Mater.* **2005**, *17*, 2194–2199; c) T.-J. Park, G. C. Papaefthymiou, A. R. Moodenbaugh, Y. B. Mao, S. S. Wong, *J. Mater. Chem.* **2005**, *15*, 2099–2105.
[16] M. Mahesh Kumar, V. R. Palkar, K. Srinivas, S. V. Suryanarayana, *Appl. Phys. Lett.* **2000**, *76*, 2764–2766.
[17] M. I. Morozov, N. A. Lomanova, V. V. Gusarov, *Russ. J. Gen. Chem.* **2003**, *73*, 1676–1680.
[18] J. K. Kim, S. S. Kim, W.-J. Kim, *Mater. Lett.* **2005**, *59*, 4006–4009.
[19] A. V. Zalesskiĭ, A. A. Frolov, T. A. Khimich, A. A. Bush, *Phys. Solid State* **2003**, *45*, 141–145.
[20] I. Sosnowska, R. Przeniosło, P. Fischer, V. A. Murashov, *J. Magn. Magn. Mater.* **1996**, *160*, 384–385.
[21] Z. V. Gabbasova, M. D. Kuz′min, A. K. Zvezdin, I. S. Dubenko, V. A. Murashov, D. N. Rakov, *Phys. Lett. A* **1991**, *158*, 491–498.
[22] M. K. Singh, H. M. Jang, S. Ryu, M.-H. Jo, *Appl. Phys. Lett.* **2006**, *88*, 042907.
[23] P. W. Voorhees, *Annu. Rev. Mater. Sci.* **1992**, *22*, 197–215.
[24] H. J. Zhou, Y. B. Mao, S. S. Wong, *Chem. Mater.* **2007**, *19*, 5238–5249.

Received: March 12, 2008
Published Online: July 4, 2008

